

Electronic Supplementary Information

Two-dimensional metal-organic polymers as cathode hybrid materials for high-performance Al-batteries

Dawid Pakulski,^{a,b*} Verónica Montes-García,^{c‡} Adam Gorczyński,^d Włodzimierz Czepa,^{b,d} Tomasz Chudziak,^{b,d} Michał Bielejewski,^e Andrzej Musiał,^e Ignacio Pérez-Juste,^f Paolo Samori,^{c*} Artur Ciesielski^{b,c*}.

^a Adam Mickiewicz University Foundation, Poznań Science and Technology Park, Rubież 46, 61-612 Poznań, Poland

^b Centre for Advanced Technologies, Adam Mickiewicz University, Uniwersytetu Poznańskiego 10, 61-614 Poznań, Poland

^c Université de Strasbourg, CNRS, ISIS 8 allée Gaspard Monge, 67000 Strasbourg, France

^d Faculty of Chemistry, Adam Mickiewicz University, Uniwersytetu Poznańskiego 8, 61-614 Poznań, Poland

^e Institute of Molecular Physics, Polish Academy of Sciences, M. Smoluchowskiego 17, 60-179 Poznan, Poland

^f Departamento Química Física, Universidade de Vigo, 36310 Vigo, Spain

E-mail: ciesielski@unistra.fr, dawid.pakulski@amu.edu.pl, samori@unistra.fr

Table of Contents

Section A. Physical characterization	S2
Section B. Electrochemical analysis	S18
Section C. Charge storage mechanism.....	S28
Section D. References.....	S34

Section A. Physical characterization

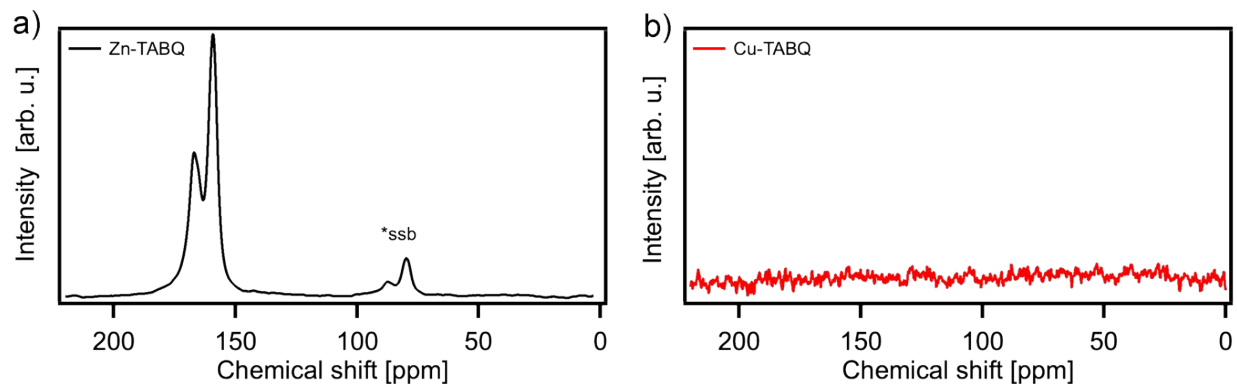


Fig. S1. C^{13} solid state NMR CP-MAS for a) Zn-TABQ and b) Cu-TABQ.

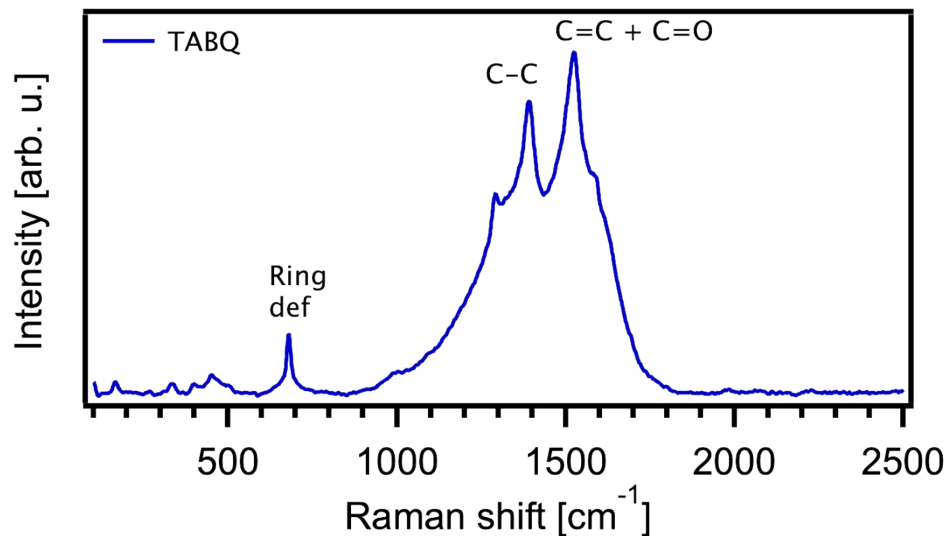


Fig. S2. Raman spectrum of TABQ.

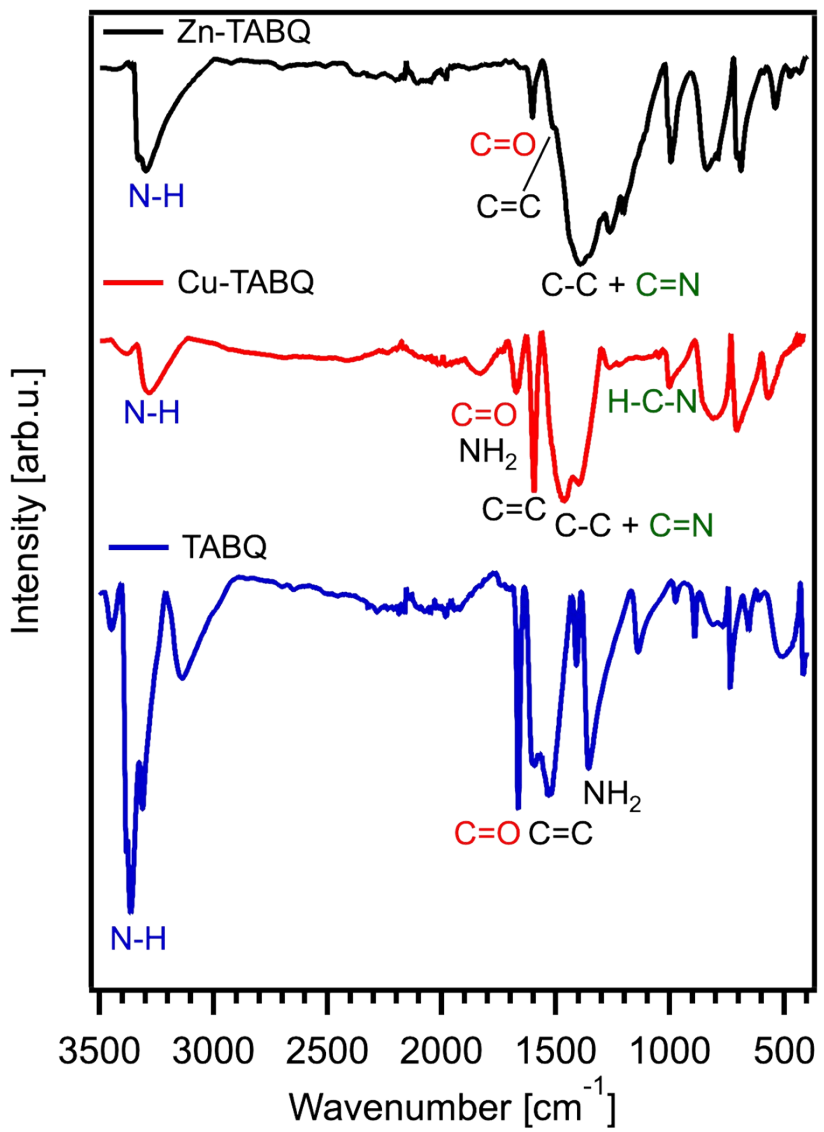


Fig. S3. FTIR spectra of Zn-TABQ (black curve), Cu-TABQ (red curve) and pure TABQ (blue curve).

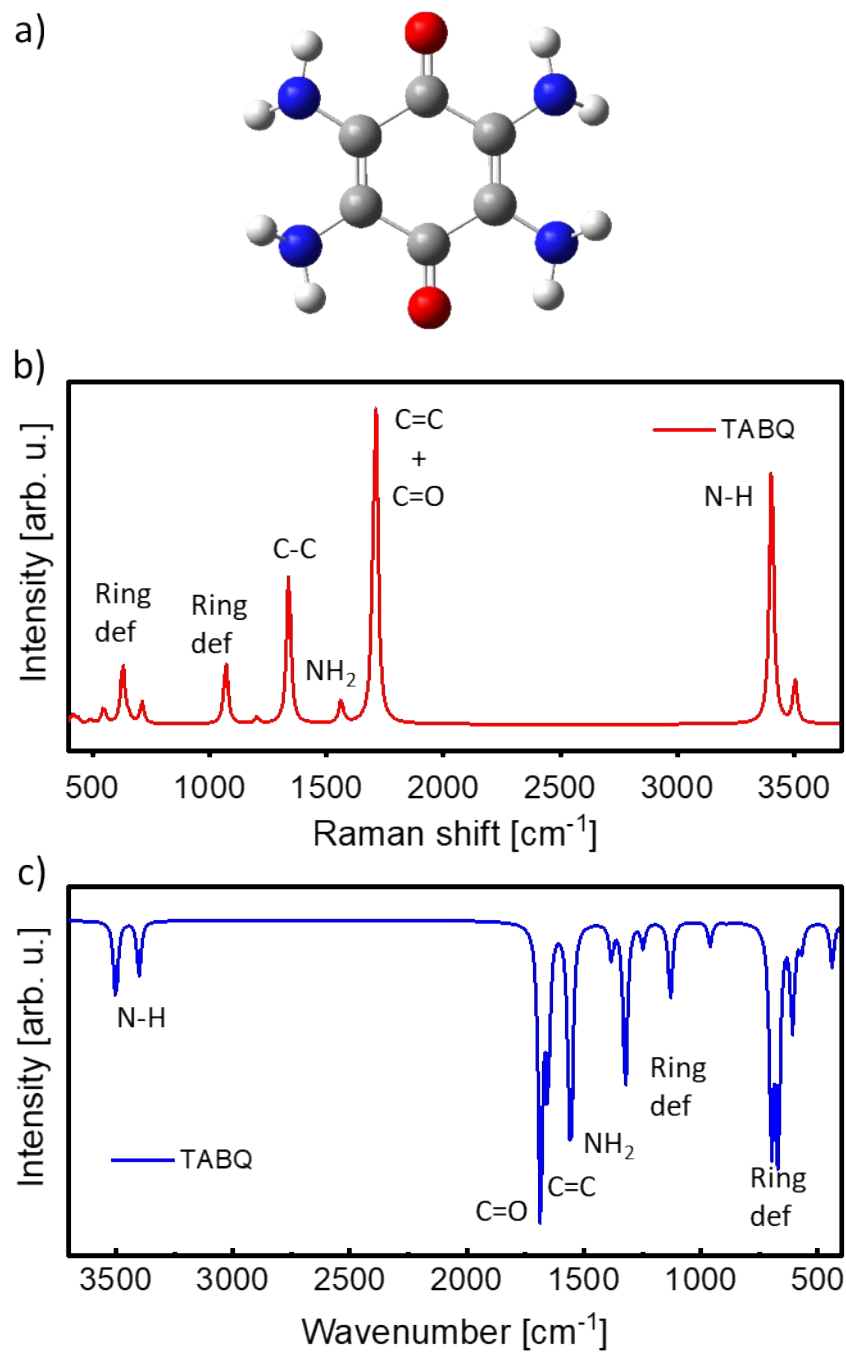


Fig. S4. a) Chemical structure of TABQ, theoretical b) Raman and c) IR spectra of TABQ.

Tab. S1. Theoretical vibrational frequencies (in cm^{-1}) for TABQ^a

Frequency (cm^{-1})	Vibrational assignments
439.0	NH ₂ twisting
570.2	Ring out-of-plane deformation + NH ₂ wagging
608.5	Ring deformation + NH ₂ wagging
628.8	Ring deformation + NH ₂ wagging
669.5	NH ₂ wagging + ring deformation
697.7	NH ₂ wagging + ring deformation
960.8	Ring deformation + NH ₂ rocking
1071.0	Ring deformation + NH ₂ rocking
1130.3	Ring deformation + NH ₂ rocking
1247.3	Ring deformation + NH ₂ rocking
1323.1	Ring deformation (asymm)
1338.4	Ring C-C stretch (symm)
1383.0	Ring C-C stretch (asymm)
1555.4	NH ₂ scissoring
1561.2	NH ₂ scissoring
1653.7	Ring C=C stretch (asymm)
1685.8	C=O stretch (asymm)
1699.9	C=O stretch (symm)
1712.4	Ring C=C stretch (symm)
3400.5	N-H stretch (symm)
3504.2	N-H stretch (asymm)

^a To analyse the assignments of theoretical vibrational frequencies it must be taken into account that the isolated molecular models of TABQ and its Zn-TABQ complex present an inversion center and, therefore, IR and Raman signals should follow the exclusion rule. As a consequence, and although our theoretical calculations were done without imposing symmetry restraints, the computed IR and Raman bands are complementary (IR signals indicated in blue color and Raman signals in red), except those corresponding to the vibrations involving the amine groups out of the molecular plane, which can be observed in both spectra (indicated in black).

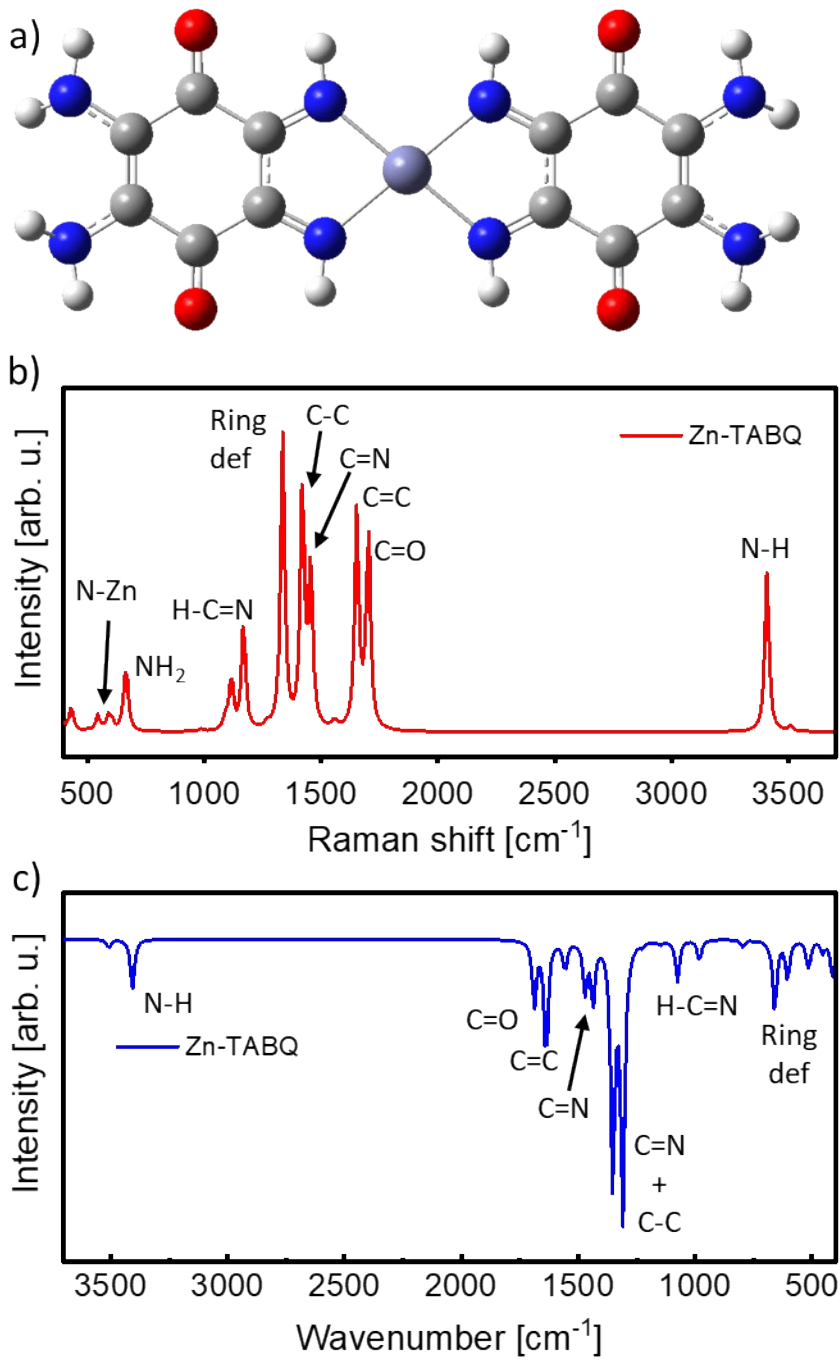


Fig. S5. a) Chemical structure of Zn-TABQ, theoretical b) Raman and c) IR spectra of Zn-TAB

Tab. S2. Theoretical vibrational frequencies (in cm^{-1}) for the Zn-TABQ complex^a

Frequency (cm^{-1})	Vibrational assignments
412.2	Ring deformation
431.4	Ring deformation
454.1	NH_2 rocking
511.7	N-Zn stretch
519.0	N-Zn stretch
544.4	N-Zn stretch
606.1	NH_2 wagging
657.2	NH_2 wagging + ring out-of-plane deformation
660.0	NH_2 wagging + ring out-of-plane deformation
660.2	Ring out-of-plane deformation
665.7	NH_2 wagging
795.6	H-N=C out-of-plane bending
981.5	H-N=C bending
1075.5	H-N=C bending
1115.6	H-N=C bending
1168.2	H-N=C bending
1309.7	Ring C=N stretch (symm) + ring C-C stretch (symm)
1334.6	Ring C-C stretch + H-N=C bending
1335.4	Ring deformation + NH_2 bendings
1337.1	Ring deformation + NH_2 bendings
1352.4	Ring C=N stretch (symm) + ring C-C stretch (asymm)
1419.8	Ring C=C stretch (symm) + H-C=N bend
1437.2	Ring C=C stretch (asymm) + H-C=N bend
1455.8	Ring C=N stretch (asymm)
1470.9	Ring C=N stretch (asymm)
1553.2	Ring C=N stretch
1555.2	NH_2 scissoring
1555.4	NH_2 scissoring
1637.5	Ring C=C stretch (symm)
1652.4	Ring C=C stretch (symm)

1686.9	C=O stretch (symm)
1702.4	C=O stretch (symm)
3407.2	NH ₂ stretch (symm) + N-H stretch (asymm)
3506.9	NH ₂ stretch (asymm)

^a To analyse the assignments of theoretical vibrational frequencies it must be taken into account that the isolated molecular models of TABQ and its Zn-TABQ complex present an inversion center and, therefore, IR and Raman signals should follow the exclusion rule. As a consequence, and although our theoretical calculations were done without imposing symmetry restraints, the computed IR and Raman bands are complementary (IR signals indicated in blue color and Raman signals in red), except those corresponding to the vibrations involving the amine groups out of the molecular plane, which can be observed in both spectra (indicated in black).

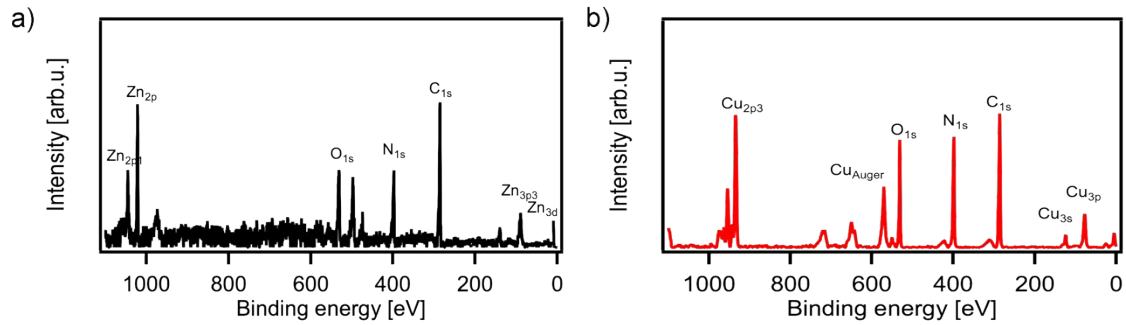


Fig. S6. XPS survey of a) Zn-TABQ and b) Cu-TABQ.

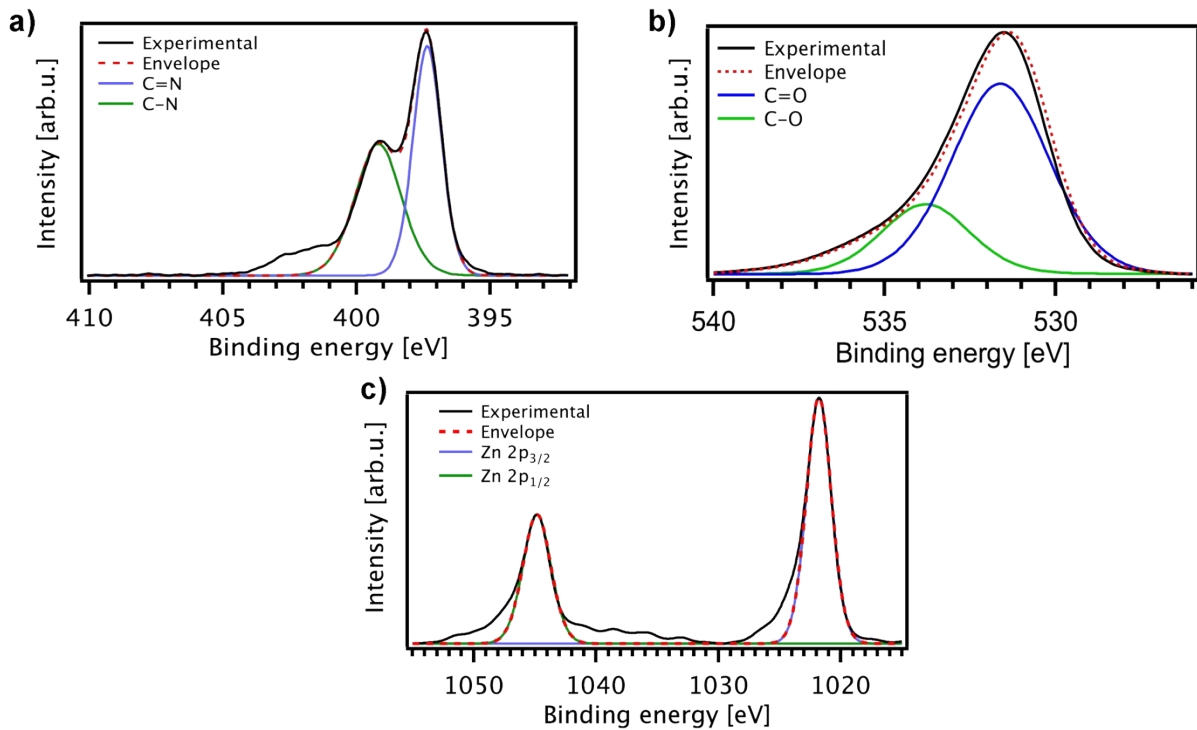


Fig. S7. XPS of Zn-TABQ a) N_{1s}, b) O_{1s}, c) Zn_{2p}.

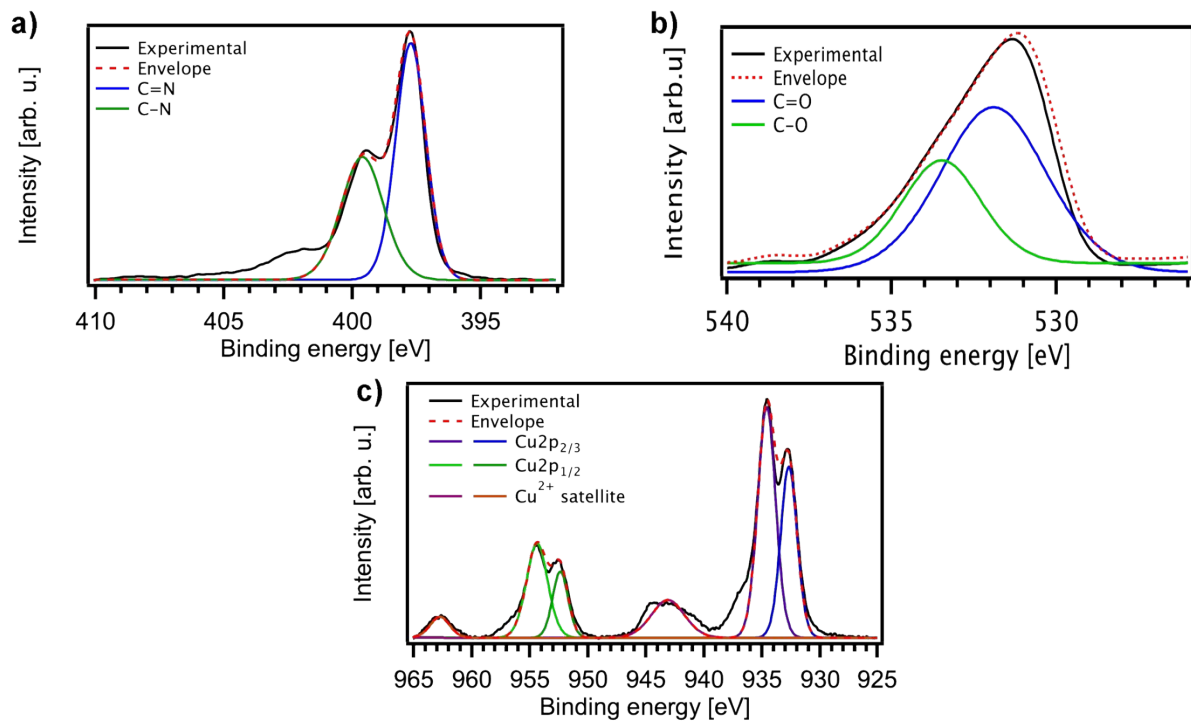


Fig. S8. XPS of Cu-TABQ a) N1s, b) O1s, c) Cu2p.

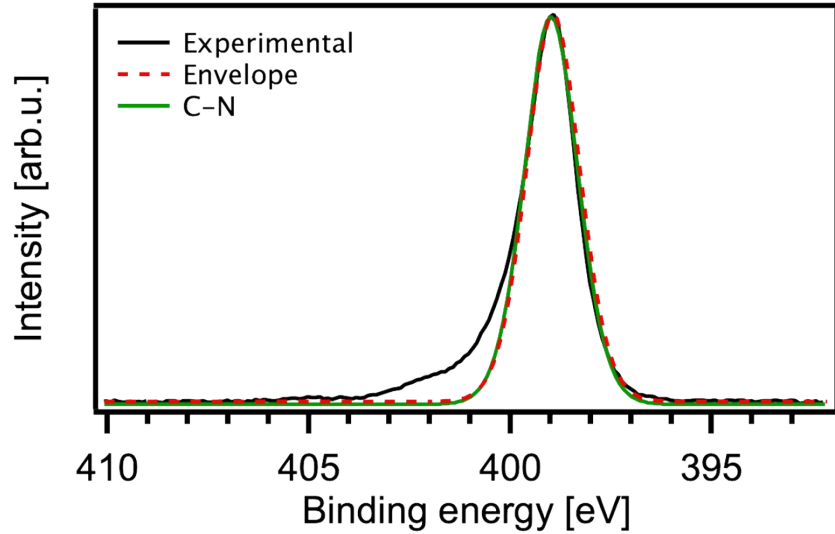


Fig. S9. N1s XPS of TABQ.

Tab. S3. Elemental analysis for Zn-TABQ.

Element	Atomic ratio [%]	Content (found) [%]	Content (calculated) [%]
C	34.9	30.94	31.40
N	23.8	24.52	24.41
O	12.0	14.07	13.94
Zn	6.0	28.76	28.49

Tab. S4. Elemental analysis for Cu-TABQ.

Element	Atomic ratio [%]	Content (found) [%]	Content (calculated) [%]
C	36.2	31.56	31.65
N	23.3	24.04	24.61
O	12.3	14.32	14.00
Cu	6.1	28.45	27.91

The atomic ratio was calculated based on experimentally content of elements.

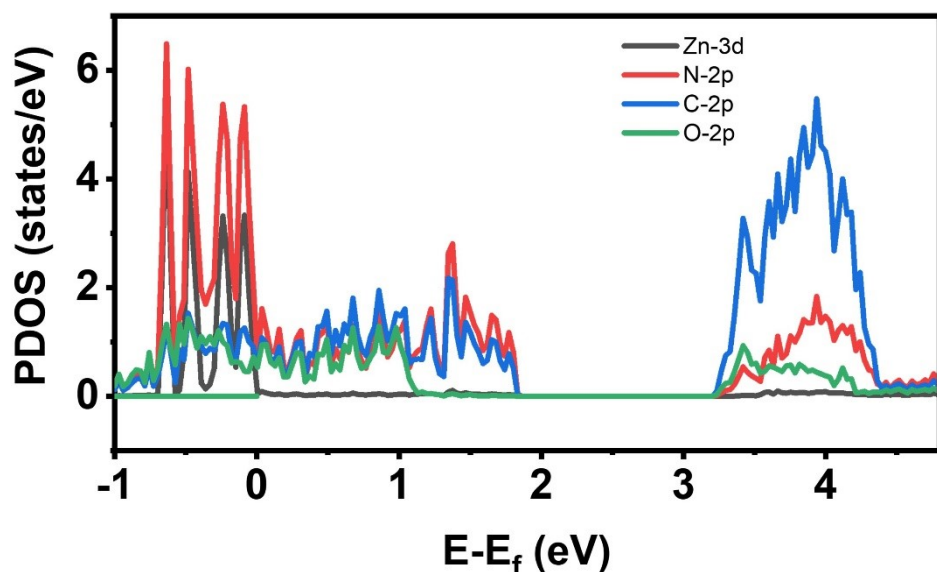
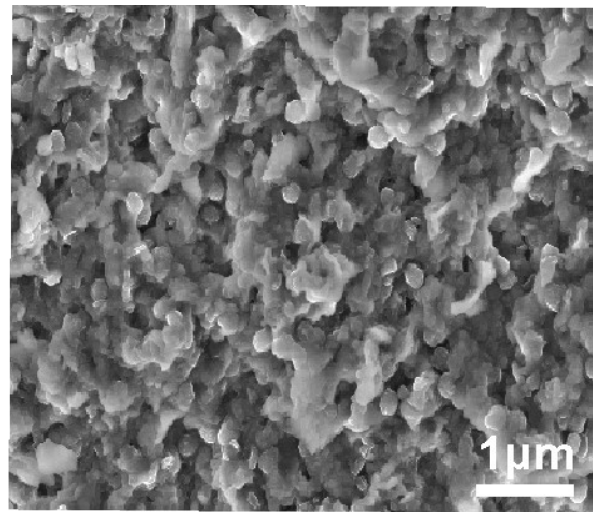


Fig. S10. SEM of pure TABQ.

Fig. S11. PDOS of selected orbitals of Zn-TABQ.

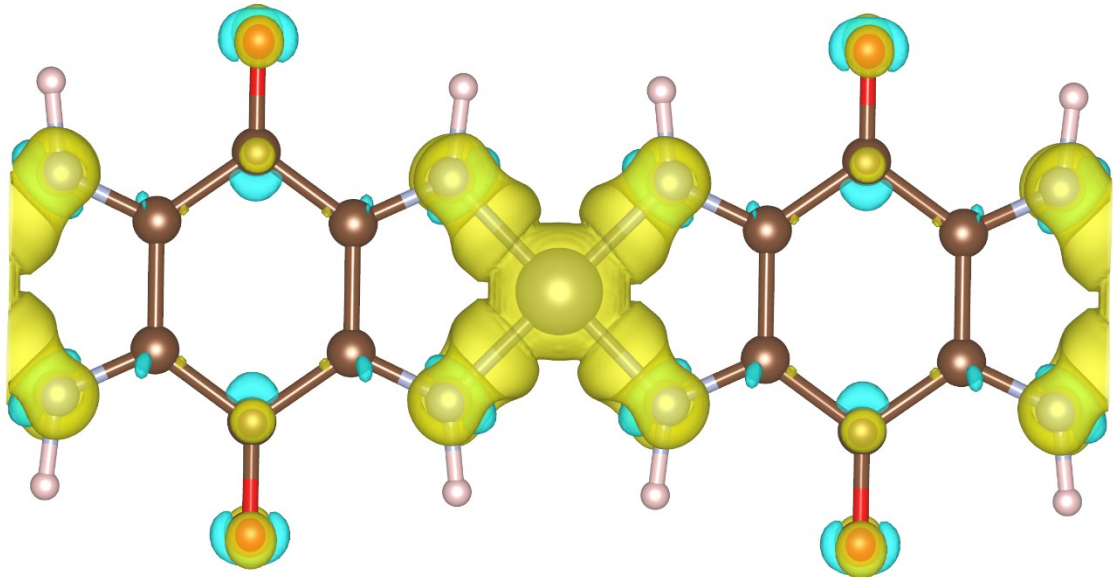


Fig. S12. Isosurface for the differential charge density of Zn-TABQ. Yellow color indicates regions where electron density increases and cyan represents regions of smaller electron density. The isosurface value is set to $0.004 \text{ e bohr}^{-3}$.

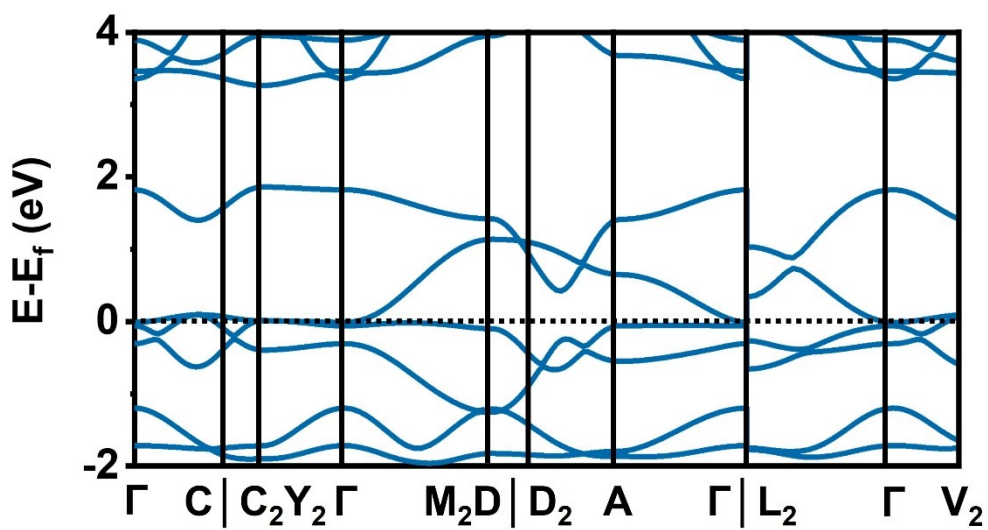


Fig. S13. Calculated electronic band structure of bulk Zn-TABQ.

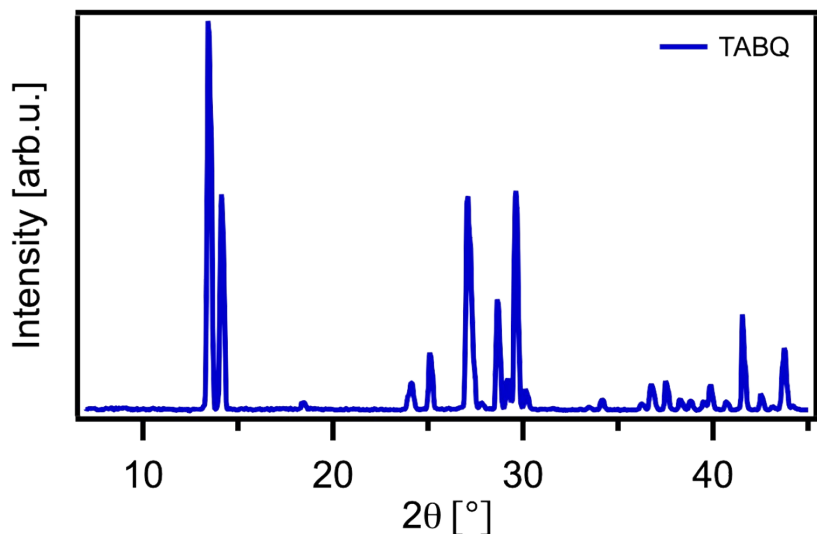


Fig. S14. PXRD for TABQ.

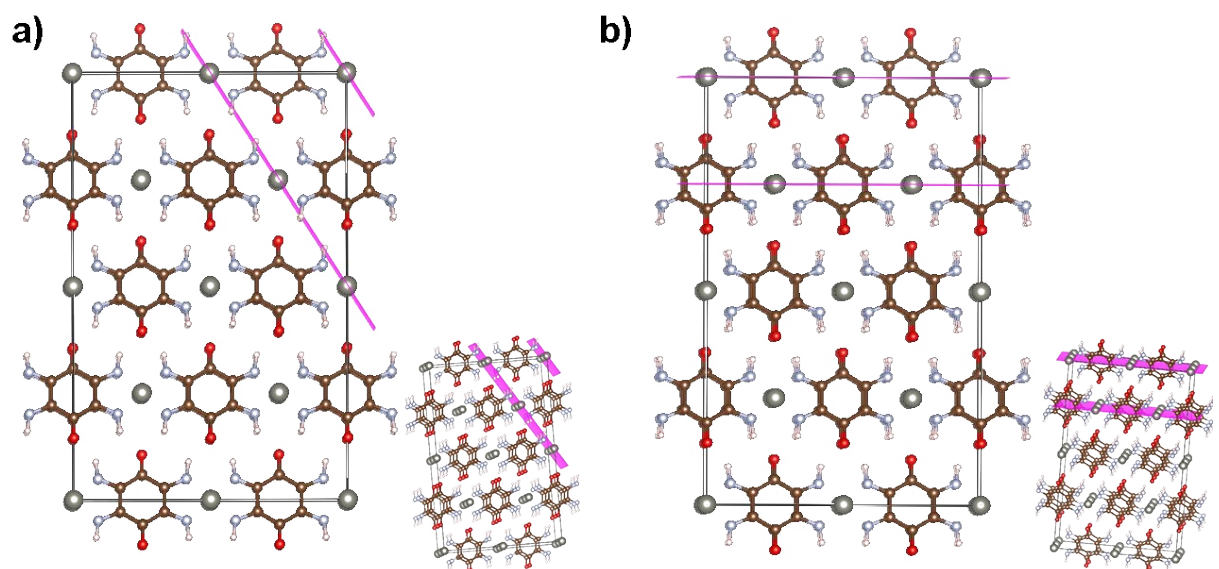


Fig. S15. Simulated structure of Zn-TABQ presented in different planes a) 110 b) 200.

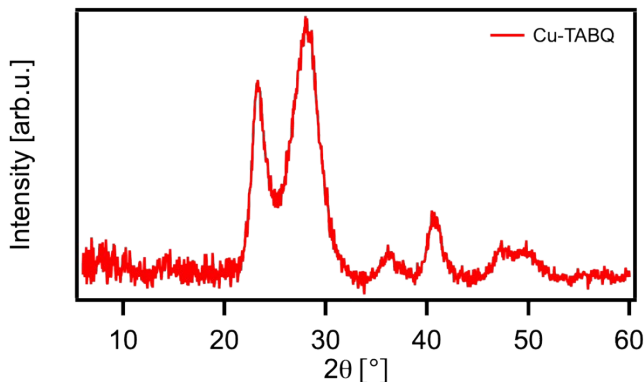


Fig. S16 PXRD spectra of Cu-TABQ

Tab. S5. D-spacing calculated for the simulated monoclinic Zn-TABQ reflections of XRD pattern.

Sample	Peak position [°]	<i>d</i> -spacing [Å]
Zn TABQ (110)	13.75	6.43±0.02
Zn TABQ (200)	14.84	5.96±0.02
Zn TABQ (001)	23.16	3.84±0.01
Zn TABQ (020)	23.26	3.82±0.02
Zn TABQ (310)	25.23	3.53±0.01
Zn TABQ (11̄1)	26.66	3.34±0.01
Zn TABQ (201)	28.33	3.15±0.01

Crystal structure of the Zn-TABQ is monoclinic, space group C 2/m, $a = 11.945 \text{ \AA}$, $b = 7.641 \text{ \AA}$, $c = 3.844 \text{ \AA}$, $\alpha = \gamma = 90.00^\circ$, $\beta = 93.24^\circ$

Tab. S6. Atomic coordinates of Zn-TABQ.

atom	site	occ.	x	y	z
C1	8j	1	0.556970	0.839200	0.896500
C5	8j	1	0.617250	0.000000	0.775400
H1	8j	1	0.678480	0.662400	0.676700
N1	4i	1	0.598500	0.678800	0.829500
O1	4i	1	0.712670	0.000000	0.574100
Zn1	2a	1	0.500000	0.500000	0.000000

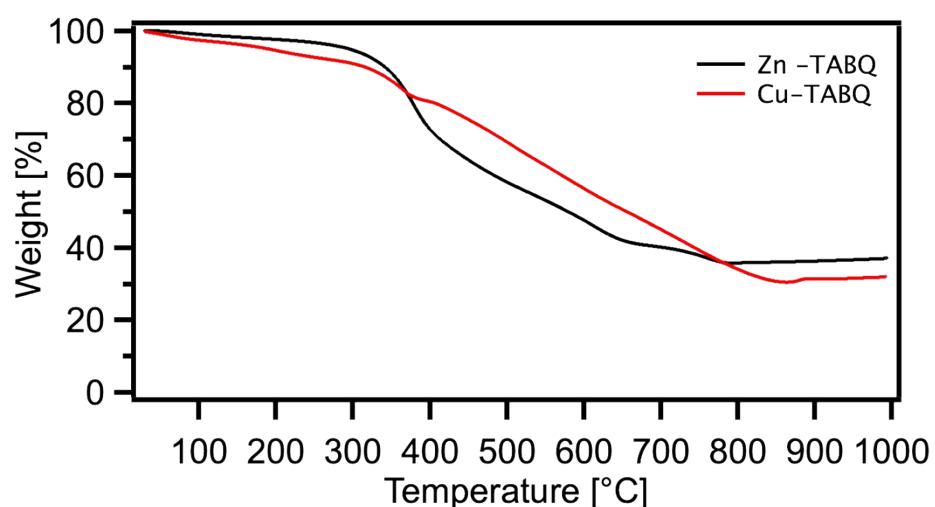


Fig. S17. TGA of Zn-TABQ (black curve) and Cu-TABQ (red curve).

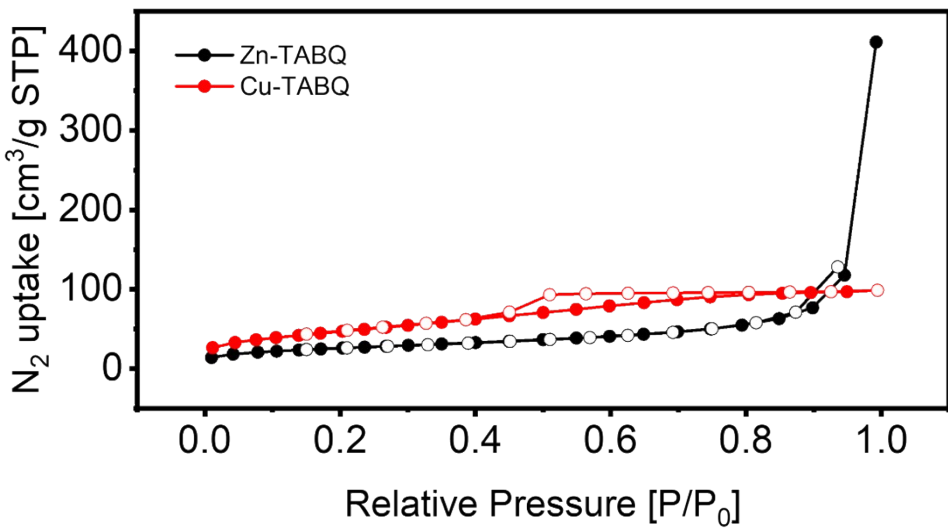


Fig. S18. BET surface area of Zn-TABQ (black curve) and Cu-TABQ (red curve).

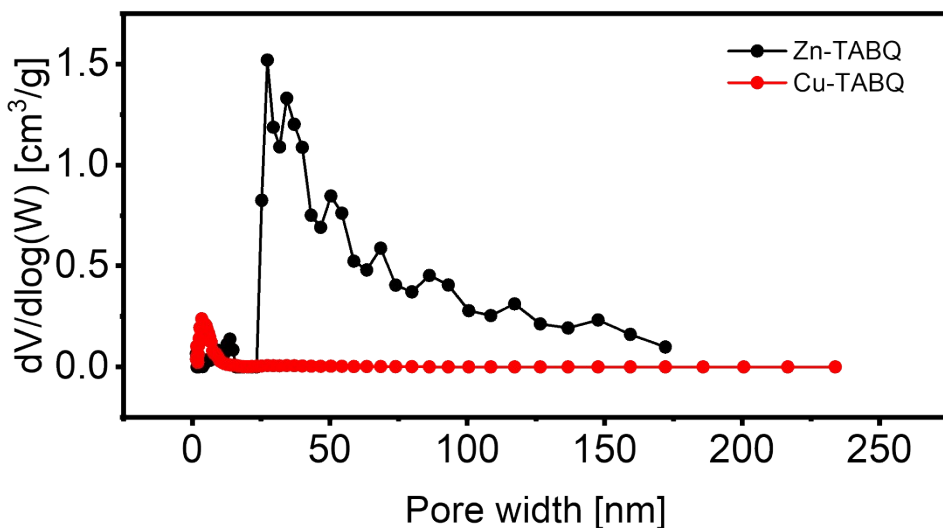


Fig. S19. Pore size distribution of Zn-TABQ (black curve) and Cu-TABQ (red curve).

Tab. S7. Parameters obtained from BET analysis

Material	Surface area (m^2/g)	Average pore volume (cm^3/g)	Average pore size (nm)
Zn-TABQ	92.079	0.666	28.952
Cu-TABQ	172.225	0.160	3.720

Section B. Electrochemical analysis

Three-electrode system

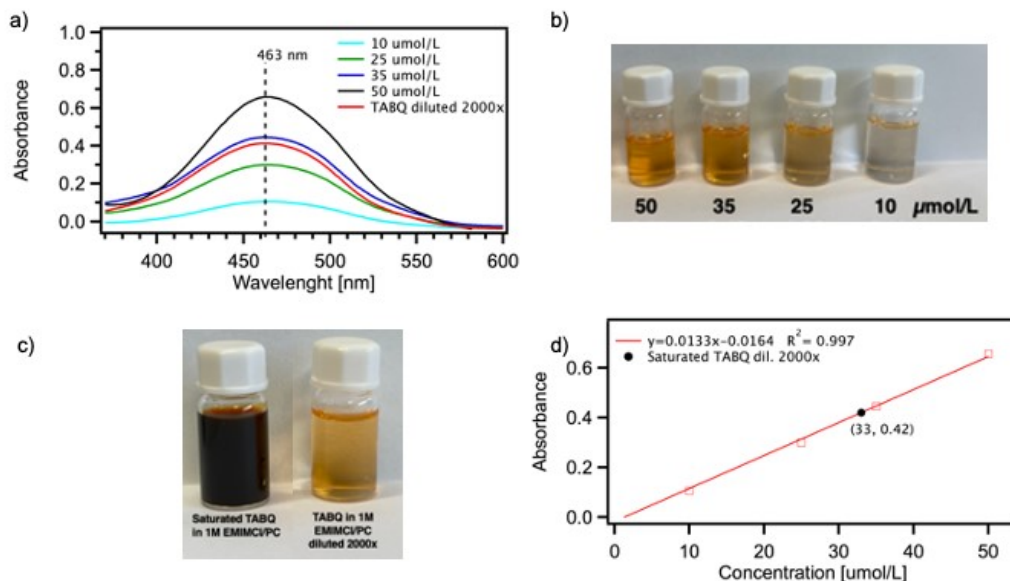


Fig. S20. a) UV-vis spectra and b, c) optical images of different concentrations of TABQ in 1M EMIMCl/PC, d) UV-vis calibration curve of TABQ in 1M EMIMCl/PC together with the calculation of the 2000 times diluted saturated solution.

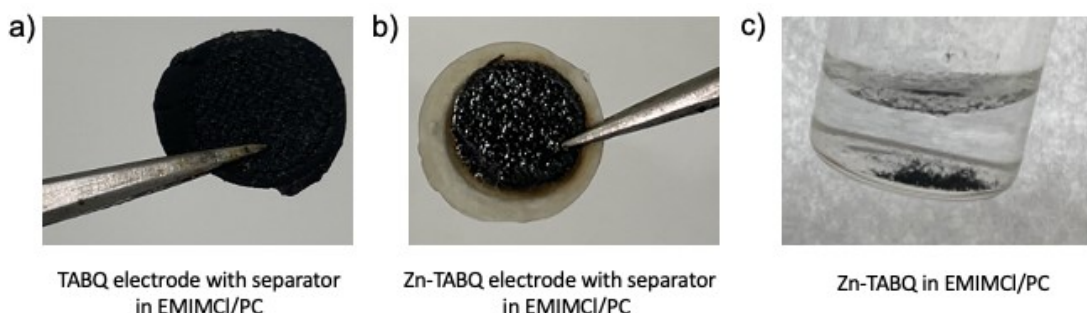


Fig. S21. Optical image of a) TABQ and b-c) Zn-TABQ electrodes with separators after their immersion in EMIMCl/PC.

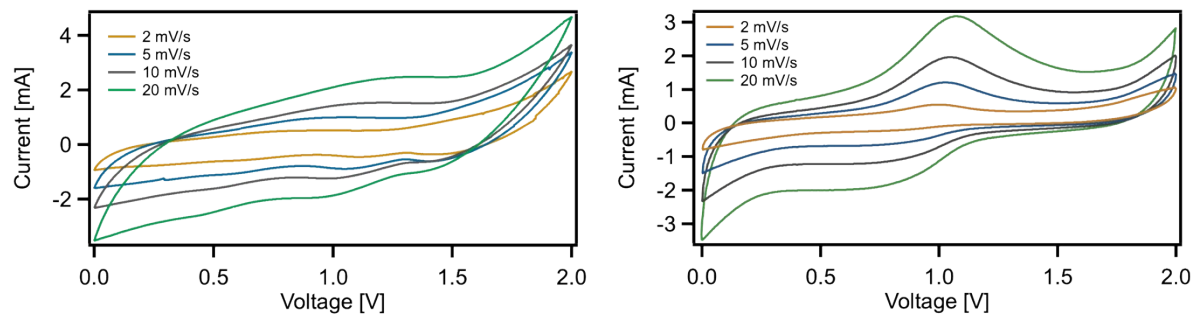


Fig. S22. CV curves of a) Zn-TABQ and b) Cu-TABQ at various scan rates.

Symmetric cells

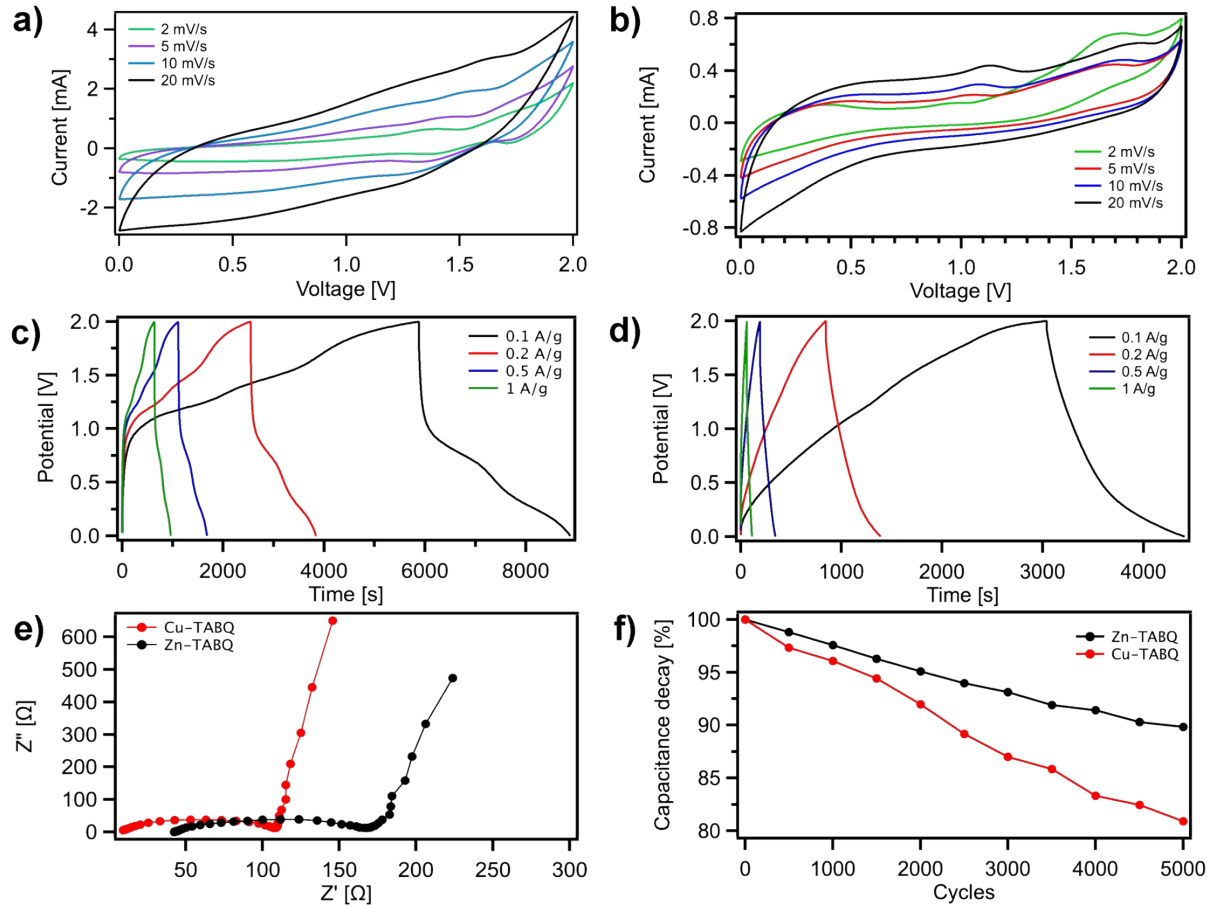


Fig. S23. Electrochemical analysis in symmetric system: a-b) CV curves at different scan rates of a) Zn-TABQ, and b) Cu-TABQ, c-d) GCD at different current densities of c) Zn-TABQ, and d) Cu-TABQ e) Nyquist plot from EIS and f) cycling stability of Zn-TABQ (black curves) and Cu-TABQ (red curves).

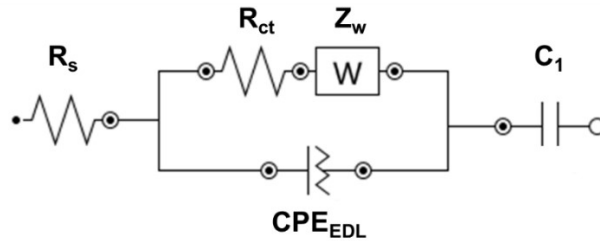


Fig. S24. The equivalent electric circuit models used for fitting the Nyquist plots.

R_s is the combined internal resistance, including the interfacial contact resistance of the material with the current collector, the ohmic resistance of electrolyte and the intrinsic resistance of the current collector, which can be obtained from the high-frequency region of the Nyquist plot by intersection on the real axis. R_{ct} is the interfacial charge transfer resistance, corresponding to the diameter of the semicircle, which represents the resistance of electrochemical reactions at the electrode surface. Furthermore, the semicircle can also reflect a constant phase element (CPE) due to the double-layer behavior. At the middle frequency region, the sloping transmission line corresponds to the Warburg element Z_w , describing the transfer and diffusion of the electrons and electrolyte ions in the pores of the electrode materials.

Tab. S8. Circuit parameters for the EIS measurements of Zn- and Cu-TABQ.

Element	Zn-TABQ		Cu-TABQ	
	Value	Estimated error (%)	Value	Estimated error (%)
R_s (Ω)	6.673	17	9.6062	7.5
R_{ct} (Ω)	83.653	2.3	97.054	1.1
Z_w ($\text{mMho s}^{1/2}$)	47.419	5	23.064	5.2
$\text{CPE}_{\text{EDL}} - Y_0$ ($\mu\text{Mho s}^N$)	$1.179 \cdot 10^{-5}$	22	9.3010^{-6}	11
$\text{CPE}_{\text{EDL}} - N$	0.89361	3.2	0.80062	1.7
C_1 (mF)	3.827	1.1	2.583	0.38
σ (S/m)	0.12	0.01	0.08	0.01

Al-batteries

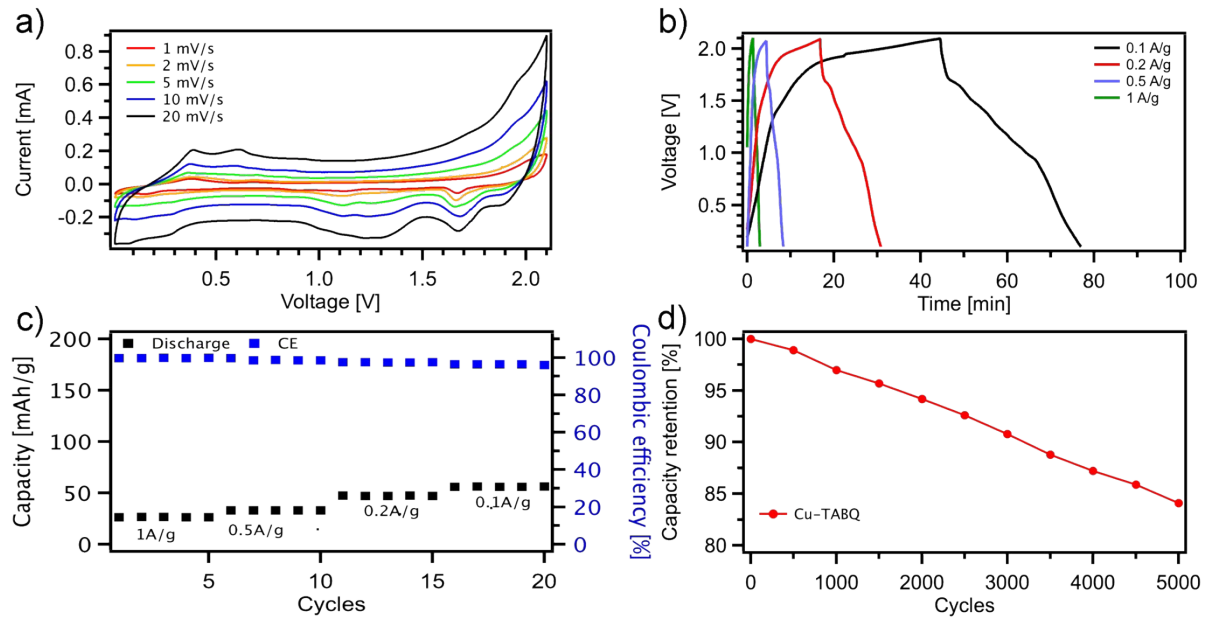


Fig. S25. Electrochemical characterization of Cu-TABQ in Al-battery configuration. a) CV curves at different scan rates, b) GCD curves at different current densities, c) specific capacity as a function of the current densities, d) cycling stability.

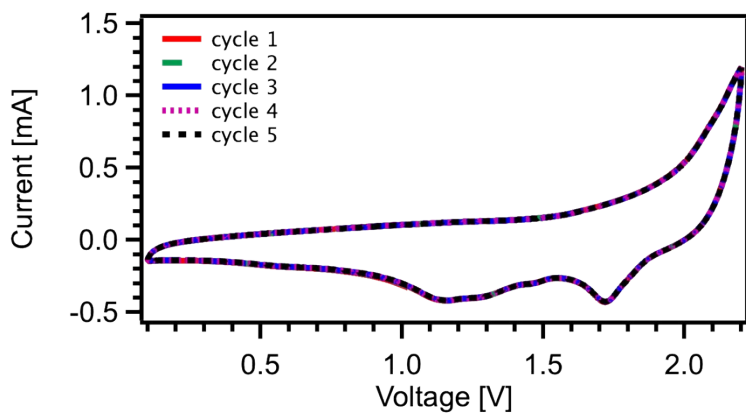


Fig. S26. Five consecutive CV curves for Zn-TABQ at a scan rate of 50 mV/s.

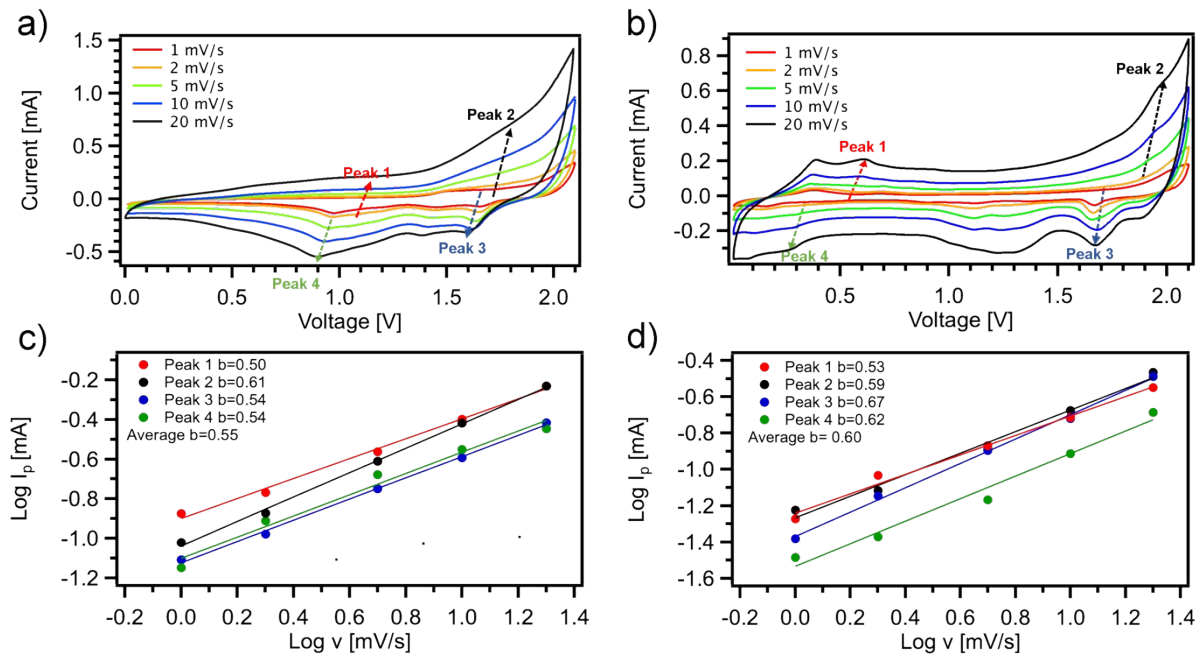


Fig. S27. Electrochemical kinetics study of Zn-TABQ and Cu-TABQ. The linear fits of $I \log v$ vs $\log v$ plots to calculate b values according to the equation of $i = av^b$ for a, c) Zn-TABQ and b, d) Cu-TABQ.

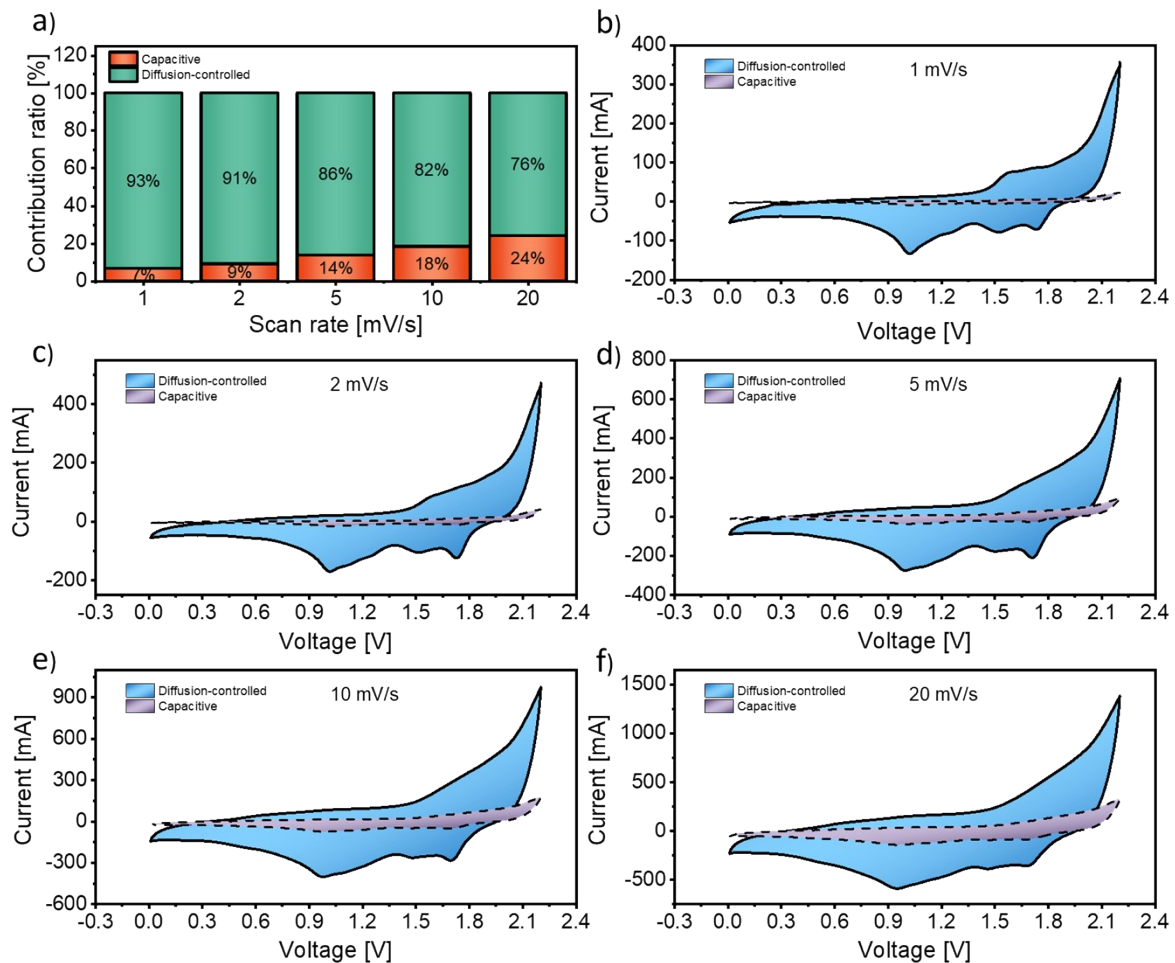


Fig. S28. a) Capacitive (contribution) and diffusion controlled contribution of Zn-TABQ. b-f) Comparison of CV curves for the capacitive contribution and diffusion-controlled contribution fraction at different scan rates for Zn-TABQ.

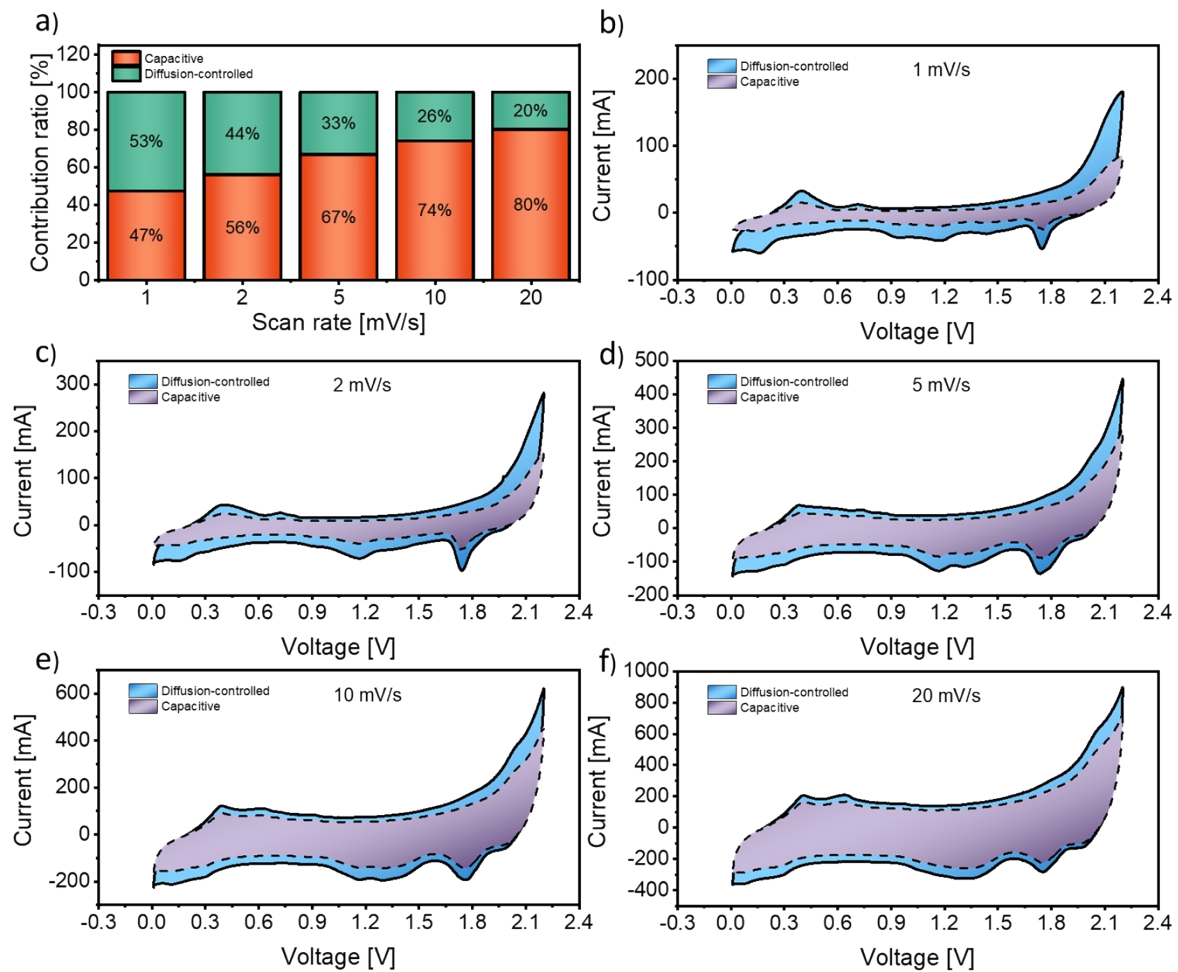


Fig. S29. a) Capacitive (contribution) and diffusion controlled contribution of Cu-TABQ. b-f) Comparison of CV curves for the capacitive contribution and diffusion-controlled contribution fraction at different scan rates for Cu-TABQ.

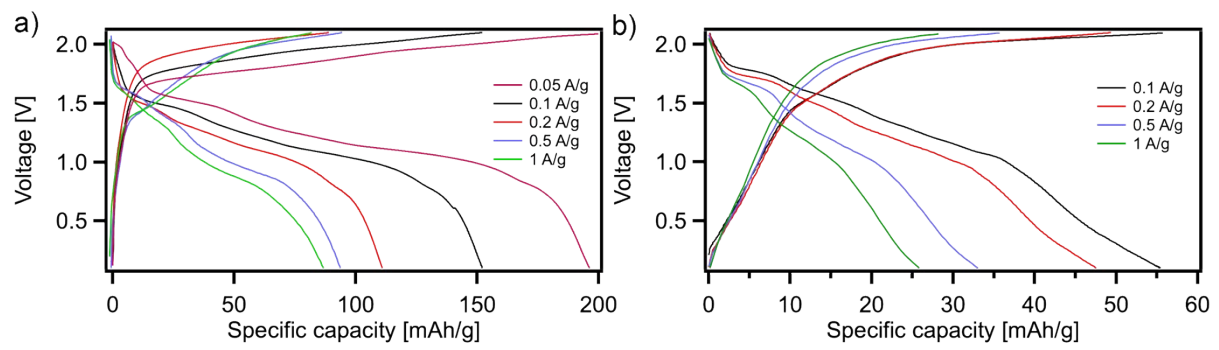


Fig. S30. Specific capacity *vs* voltage for a) Zn-TABQ and b) Cu-TABQ at different current densities

Table S9. State of the art of the electrochemical performance of different cathode materials in Al-batteries.

Cathode	Electrolyte	Capacity [mAh/g]	Current [A/g]	Voltage window [V]	Stability/ cycles	Power density [kW/kg]	Energy density [Wh/kg]	Ref.
Zn-TABQ	AlCl ₃ /EMIMCl	198	0.05	2.1	5000 - 92%	1.01	247	This work
Cu-TABQ	AlCl ₃ /EMIMCl	57	0.1	2.1	5000 – 84%	0.91	63	This work
Al-(N4) _n	AlCl ₃ /EMIMCl	135	0.1	1.1	4000	-	35.6	¹
PQ-Δ	AlCl ₃ /EMIMCl	95	0.2	1.4	5000	1.05	50	²
Phenanthrenequinone (PQ)	AlCl ₃ /EMIMCl	100	1	1.1	8000 – 90%	-	53	³
Phenanthrenequinone infiltrated with activated carbon (AC(PQ))	AlCl ₃ /EMIMCl	123	0.1	1.25	8000	0.4	49	³
Self-protonated Polyaniline (PANI-H)	AlCl ₃ /EMIMCl	120	6	1.1	8000 – 87.6%	-	-	⁴
Protonated polyaniline/single-walled carbon nanotubes composite (PANI/SWCNTs)	AlCl ₃ /EMIMCl	130	4	1.05	8000	9.35	30	⁴
Anthraquinone (AQ)	AlCl ₃ /EMIMCl	100	0.25	1.05	500	1.79	72	⁵
Anthracene-9,10-dione (AQ)	AlCl ₃ /EMIMCl	170	0.1	0.75	160	0.1	16	⁶
Polythiophene (PT)	AlCl ₃ /EMIMCl	88	0.016	1.4	100 - 80%	-	44.4	⁷
Poly(nitropyrene-co-pyrene) (PNP)	AlCl ₃ /EMIMCl	100	0.2	1.7	1000 – 80%	-	-	⁸
tetracyanoquinodimethane(TCNQ)	AlCl ₃ /EMIMCl	180	0.5	1.4	2000 - ~100%	1.2	43	⁹

1,10 -phenanthroline -5,6 - dione (MN)	AlCl ₃ /EMIMCl	121	0.1	1.55	200	0.26	32	6
Phenanthrene -9,10 -dione (M)	AlCl ₃ /EMIMCl	134	0.1	1.3	160	0.2	27	6
2,3,5,6-tetraphthalimido-1,4- benzoquinone (TPB)	AlCl ₃ /EMIMCl	175	0.1	2.4	250 – 90%	-	-	6
2,3,5,6 -tetraphthalimido - p - benzoquinone (TPBQ)	AlCl ₃ /EMIMCl	177	0.02	1.2	3000	0.04	37	10
5,10,15,20 - tetraphenylporphyrin (H ₂ TPP)	AlCl ₃ /EMIMCl	101	0.1	1.3	5000	0.35	35	11

Section C. Charge storage mechanism

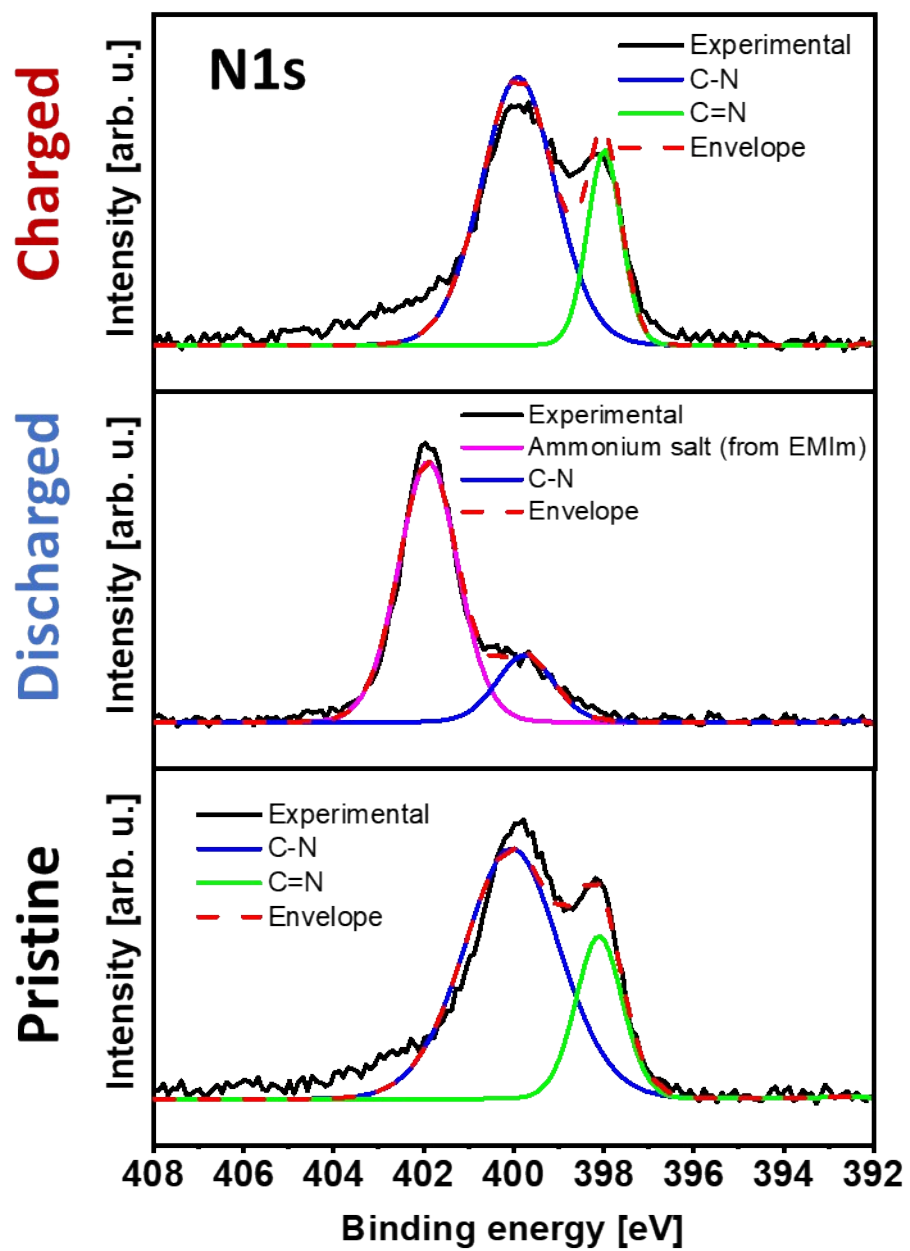


Fig. S31. Deconvolution of N1s spectra of Zn-TABQ in pristine, discharged and charged form.

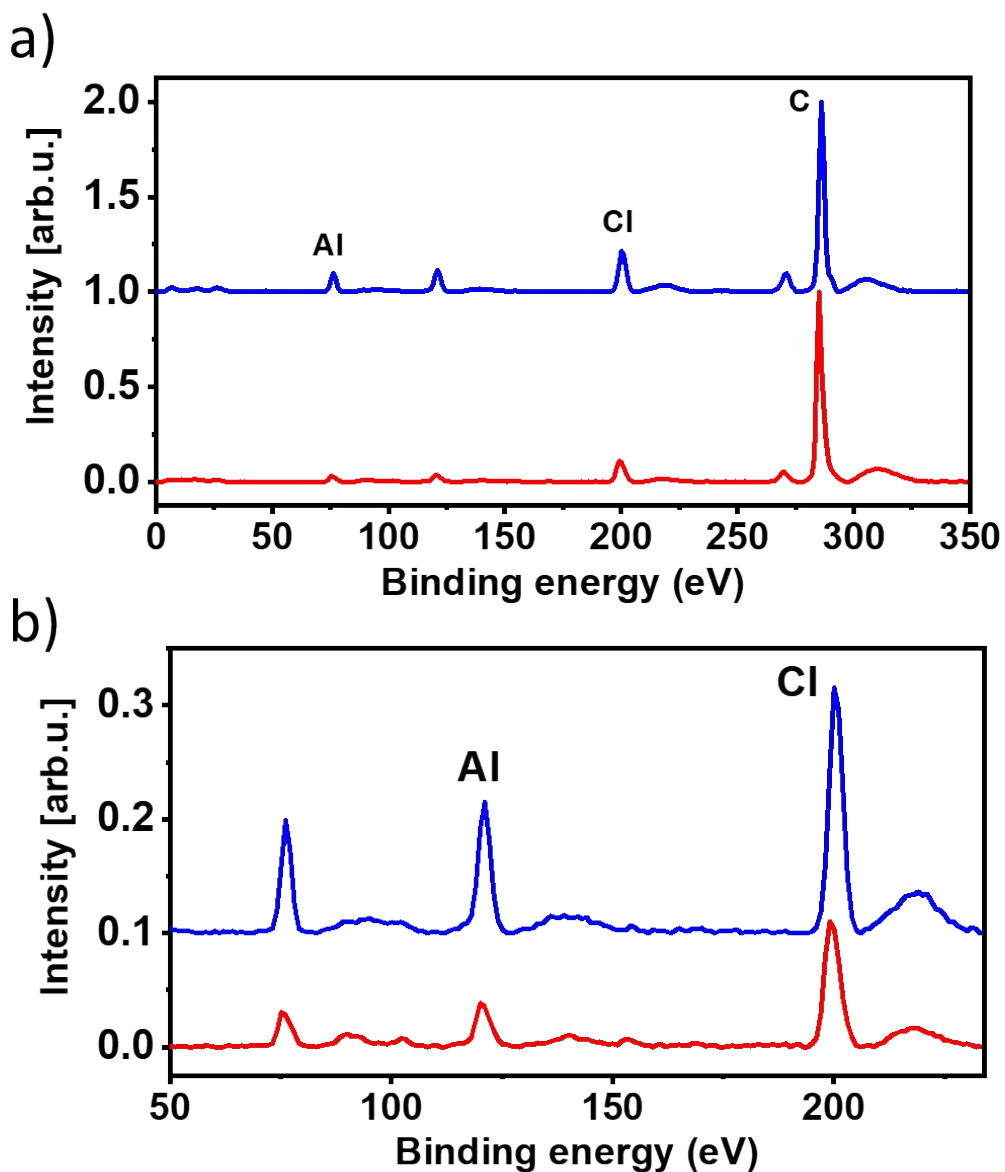


Fig. S32. Survey spectra of Zn-TABQ in the charged (red) and discharged (blue) states normalized by the carbon signal. a) full range and b) magnification of the Al and Cl signals.

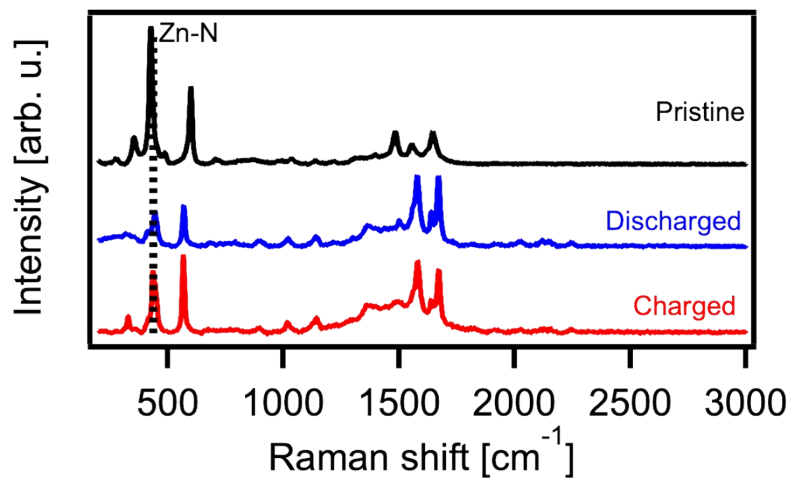


Fig. S33. Raman spectra of Zn-TABQ in pristine, discharged and charged form.

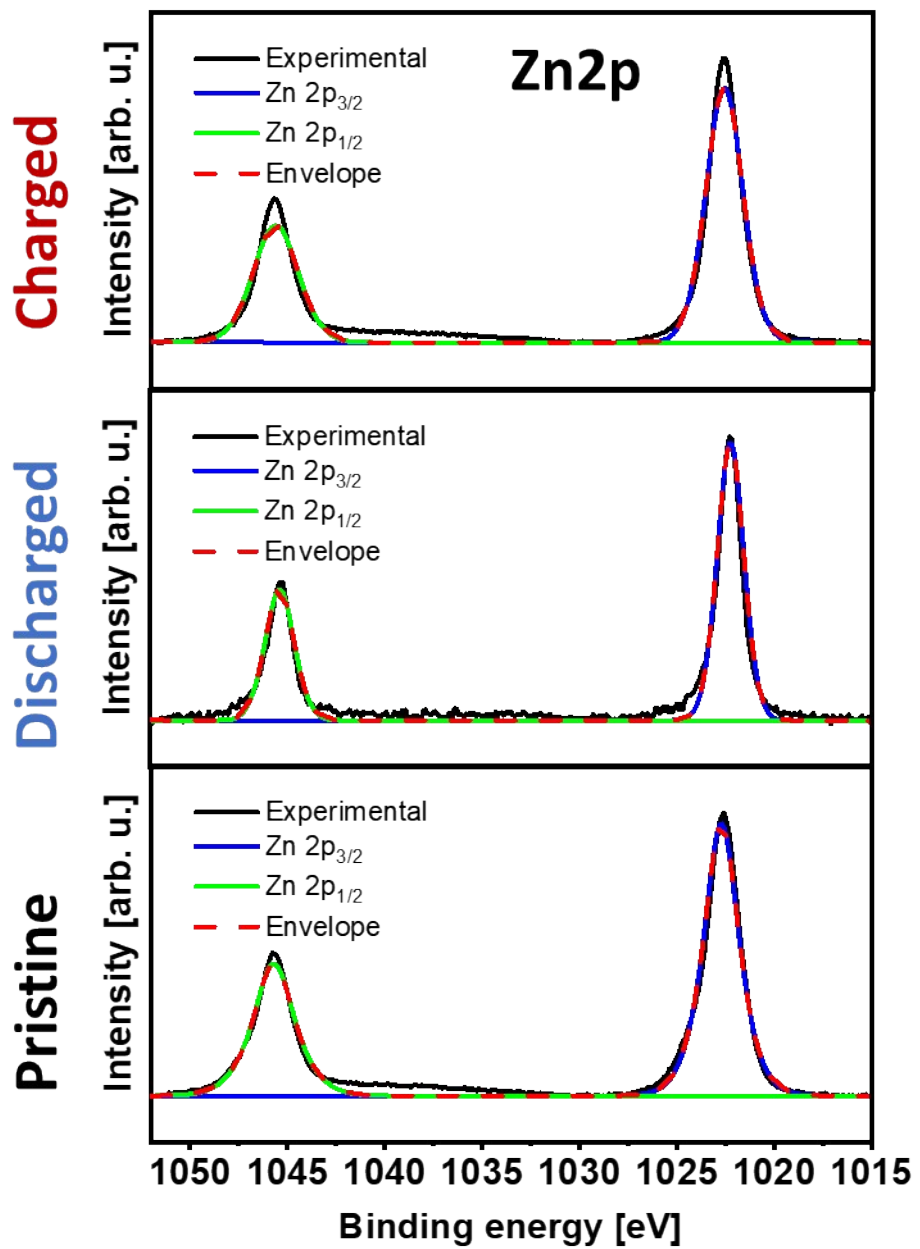


Fig. S34. Zn2p XPS spectra of Zn-TABQ in pristine, discharged and charged form.

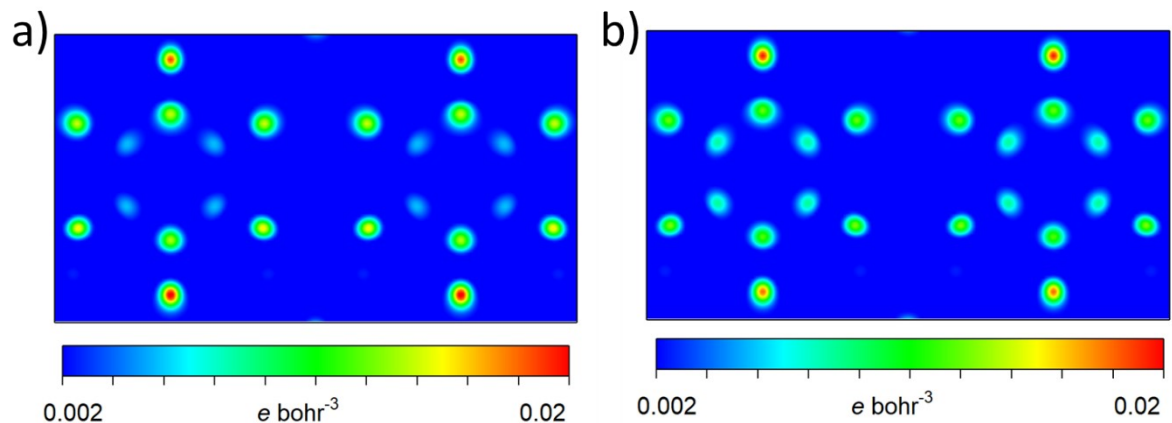


Fig. S35. Successive charge density changes after the addition of two electron (a) and four electrons (b) to a Zn-TABQ unit.

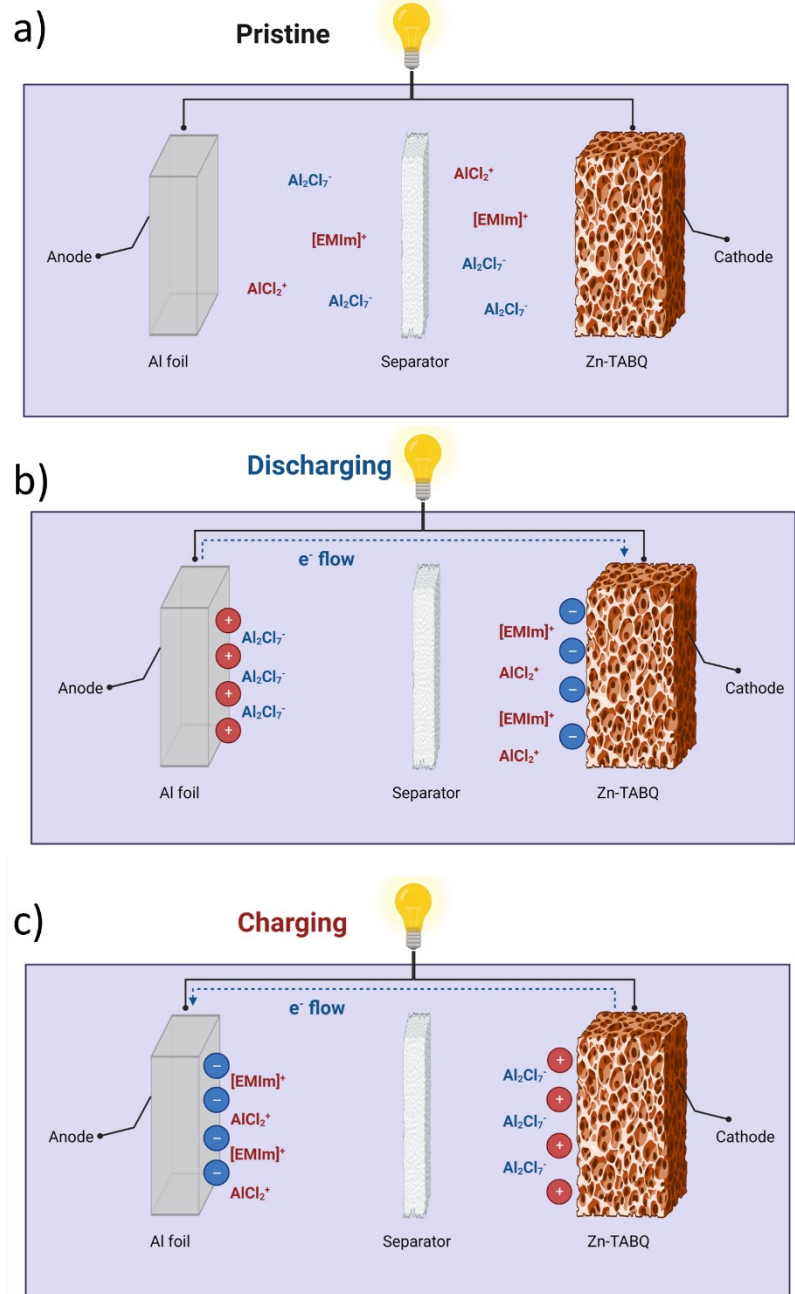


Fig. S36. Schematic diagram of the Al battery using Zn-TABQ as cathode.

Section D. References

1. G. Wang, E. Dmitrieva, B. Kohn, U. Scheler, Y. Liu, V. Tkachova, L. Yang, Y. Fu, J. Ma, P. Zhang, F. Wang, J. Ge and X. Feng, *Angew. Chem., Int. Ed. Engl.*, 2022, **61**, e202116194.
2. D. J. Kim, D.-J. Yoo, M. T. Otley, A. Prokofjevs, C. Pezzato, M. Owczarek, S. J. Lee, J. W. Choi and J. F. Stoddart, *Nat. Energy*, 2019, **4**, 51-59.
3. D.-J. Yoo and J. W. Choi, *J. Phys. Chem. Lett.*, 2020, **11**, 2384-2392.
4. S. Wang, S. Huang, M. Yao, Y. Zhang and Z. Niu, *Angew. Chem., Int. Ed. Engl.*, 2020, **59**, 11800-11807.
5. J. Bitenc, N. Lindahl, A. Vizintin, M. E. Abdelhamid, R. Dominko and P. Johansson, *Energy Storage Mater.*, 2020, **24**, 379-383.
6. N. S. Hudak, *J. Phys. Chem. C*, 2014, **118**, 5203-5215.
7. M. Walter, K. V. Kravchyk, C. Böfer, R. Widmer and M. V. Kovalenko, *Adv. Mater.*, 2018, **30**, 1705644.
8. H. Lu, F. Ning, R. Jin, C. Teng, Y. Wang, K. Xi, D. Zhou and G. Xue, *ChemSusChem*, 2020, **13**, 3447-3454.
9. Y.-T. Kao, S. B. Patil, C.-Y. An, S.-K. Huang, J.-C. Lin, T.-S. Lee, Y.-C. Lee, H.-L. Chou, C.-W. Chen, Y. J. Chang, Y.-H. Lai and D.-Y. Wang, *ACS Appl. Mater. Interfaces*, 2020, **12**, 25853-25860.
10. M. Mao, Z. Yu, Z. Lin, Y.-S. Hu, H. Li, X. Huang, L. Chen, M. Liu and L. Suo, *J. Mater. Chem. A*, 2020, **8**, 23834-23843.
11. X. Han, S. Li, W.-L. Song, N. Chen, H. Chen, S. Huang and S. Jiao, *Adv. Energy Mater.*, 2021, **11**, 2101446.